AD-A067 173 HAWAII UNIV HONOLULU DEPT OF PHYSICS AND ASTRONOMY F/G 20/2
A STUDY OF THE ACOUSTO-OPTIC EFFECT IN NEMATICS AS A MEANS OF A--ETC(U)
MAR 79 C F HAYES N00014-78-C-0417
UNCLASSIFIED TR-002 NL

| OF |
AD
A067173

END
DATE
FILMED
6-79
DDC

Unclassified

SECURITY CLASSIFICATION OF THIS PAGE (When Data Entered)

REPORT DOCUMENTATION PAGE

READ INSTRUCTIONS BEFORE COMPLETING FORM

1. REPORT NUMBER	2. GOVT ACCESSION NO.	3. RECIPIENT'S CATALOG NUMBER
(14) TR-002	(12)	

4. TITLE (and Subtitle)

(6) A STUDY OF THE ACOUSTO-OPTIC EFFECT IN NEMATICS AS A MEANS OF ACOUSTIC FIELD IMAGING.

5. TYPE OF REPORT & PERIOD COVERED: Technical (March, 1979)

6. PERFORMING ORG. REPORT NUMBER

7. AUTHOR(s)

(10) Charles F. Hayes (Principal Investigator)

8. CONTRACT OR GRANT NUMBER(s)

(15) N00014-78-C-0417

9. PERFORMING ORGANIZATION NAME AND ADDRESS

Department of Physics and Astronomy
University of Hawaii
Honolulu, Hawaii 96822

10. PROGRAM ELEMENT, PROJECT, TASK AREA & WORK UNIT NUMBERS

121108

11. CONTROLLING OFFICE NAME AND ADDRESS

Office of Naval Research
Department of the Navy
Arlington, Virginia 22217

(11) 8 March 1979

30

14. MONITORING AGENCY NAME & ADDRESS (if different from Controlling Office)

(12) 31 p.

15. SECURITY CLASS. (of this report)

LEVEL II

15a. DECLASSIFICATION/DOWNGRADING SCHEDULE

16. DISTRIBUTION STATEMENT (of this Report)

Approved for public release; distribution unlimited.

(9) Technical rept.

17. DISTRIBUTION STATEMENT (of the abstract entered in Block 20, if different from Report)

DDC RECEIVED APR 10 1979 C

18. SUPPLEMENTARY NOTES

19. KEY WORDS (Continue on reverse side if necessary and identify by block number)

Acoustic Streaming
Nematic
Acousto-Optic Effect
Acoustic Imaging

This contract studied

20. ABSTRACT (Continue on reverse side if necessary and identify by block number)

The program of this contract has been to study the acousto-optic effect which occurs in nematic liquid crystals when excited by acoustic waves including extension and testing of the streaming model developed by C.F. Hayes. The results indicate that the model is valid. Equations have been solved giving both the magnitudes and patterns of the induced flows. These results have been tested experimentally and agree quite well with the theory.

DD FORM 1 JAN 73 1473 EDITION OF 1 NOV 65 IS OBSOLETE S/N 0102-014-6601

Unclassified

SECURITY CLASSIFICATION OF THIS PAGE (When Data Entered)

403 697

AD A067173

DDC FILE COPY

Technical Report: 002

A Study of the Acousto-Optic Effect in Nematics as a Means of Acoustic Field Imaging

C. F. Hayes

Department of Physics and Astronomy

University of Hawaii

Honolulu, Hawaii 96822

March 1979

I. INTRODUCTION

The fact that acoustic waves could give optical effects in nematic liquid crystals has been known since 1936. In that year Fredericks and Zolin[1] excited a nematic liquid crystal by tuning forks of 200 to 600 Hz while making optical observations with crossed polarizers. It was not until 1969 that Fergason[2] suggested that a liquid crystal device may be made for detecting acoustic intensity. Since 1970 there have been approximately forty research articles published in this area. However, the basic mechanism causing the effect was not understood until the last three years. Differential acoustic absorption,[3] transverse second-order stress,[4] cybotactic groups,[5] the piezoelectric effect[6] and anisotropy of acoustic speed have all been proposed to be the mechanism for the effect. In the early work, both experimental and theoretical, a threshold of acoustic intensity was reported to be required. In 1976, three groups: Sripaipan, Hayes, Fang;[7] Candau, Peters, Nagai;[8] and Dion, DeForest;[9] reported that there is in fact no threshold for the effect. The former two groups attributed the effect to acoustic streaming. Further, whereas all of the previous work had required some special property of a liquid crystal for the effect acoustic streaming would result in any viscous liquid. It is simply that acoustic streaming or any flow in a liquid crystal results in optical effects. The streaming theory has been extended to include the simultaneous effect of an electric field by Hayes[10] in 1978. Again the streaming model successfully explained the experimental results. The logical result of the streaming explanation is that a cell to visualize an acoustic field could be made by separating the liquid crystal into distinct regions to confine the flow. Nagai and Iizuka[11,12] have made such a device. However, there has not been a direct observation of the flows induced in these cells nor quantitative

theoretical work performed giving the speeds of flow or the flow patterns in the cell. It is the goal of this report to provide direct evidence for the flows. In Section II a theory is presented which predicts the magnitude of the flow speed and the form of the flow pattern one would expect in a viscous fluid. In Section III results are presented for observations of these fluid flows.

II. THEORY OF FLUID MOTION

A. Non-viscous Limit

We will develop equations describing the motion induced in a disc shaped liquid bound between two solids. The solid surfaces are assumed planar with an ultrasonic wave traveling from one solid, through the fluid and on through the second solid. We will take the cylindrical boundary of the disc to be open to a gas of negligible density. Such a system could be made by placing a drop of water between two glass microscope slides. We will further take the distance between the planes, the height of the disc, to be smaller than the wavelength of the ultrasonic wave. The oscillatory motion of the wave will produce a static flow in the fluid, acoustic streaming. We will find the form of the resulting flow patterns and the magnitude of the fluid speed.

In order to understand the approximations which must be made to obtain a tractable solution we will first investigate a simpler problem where viscosity is omitted and the disc is assumed of infinite height.

Consider a column of non-viscous fluid with equilibrium density ρ_o supported by a piston. See Figure 1. We assume the piston-fluid interface is located at $z = 0$ and take the radius of the fluid to be R. The result of the piston's velocity, $Ae^{-i\omega t}$, is a compression wave which propagates along the cylindrical axis of the column, the positive z axis. Because of the boundary at $r = R$ there will also be laterally induced waves as well. The equation describing the pressure, P, in the column is

$$\nabla^2 P = \frac{1}{C^2} \frac{\partial^2 P}{\partial t^2} \tag{1}$$

where C is the speed of the wave in the fluid. At $r = R$ we must have $P = 0$. The solution to Eq. 1 satisfying this boundary condition is

$$P = \sum_n A_n J_o (k_n r) e^{i k_n'' z - i\omega t} \tag{2}$$

where $J_o( )$ is the Bessel function of order zero,

$$k_n^2 = \frac{\omega^2}{C^2} - k_n''^2 \tag{3}$$

and

$$\alpha_n = k_n R = 2.405, 5.520, 8.654, 11.792, \ldots \tag{4}$$

where

$$J_o(\alpha_n) = 0 \qquad n = 0, 1, 2, \ldots \tag{5}$$

The partial differential equation relating the pressure to $\vec{v}$, the fluid velocity is given by

$$\rho_o \frac{\partial \vec{v}}{\partial t} = - \nabla P \tag{6}$$

We have at z = 0 the further boundary condition:

$$v_z = A e^{-i\omega t} \tag{7}$$

Combining Eq's. 2, 6, and 7 we have

$$\rho_o \omega A = \sum_n A_n k_n'' J_o (k_n r) \tag{8}$$

Operating on both sides of Eq. 8 with $\int_o^1 \frac{r}{R} J_o \left(\alpha_m \frac{r}{R}\right) d\left(\frac{r}{R}\right)$ we obtain

$$A_n = \frac{2\rho_o \omega A}{\alpha_n k_n'' J_1 (\alpha_n)} \tag{9}$$

Now solving Eq. 6 for v_r and taking r = R we find

$$v_R = \sum_n \frac{2i A}{R k_n''} e^{i k_n'' z - i\omega t} \tag{10}$$

From Eq. 3 and 4 we see the value of R may be adjusted with respect to λ to give $k_n'' = 0$. This condition gives a resonance and may occur for modes $n = 0, 1, 2, \ldots$. The corresponding values of R are:

$$R = .383\ \lambda,\ .879\ \lambda,\ 1.38\ \lambda,\ 1.88\ \lambda,\ \ldots \tag{11}$$

Figure 2 shows the amplitudes of v_R/A at $z = 0$ as a function of R/λ for modes $n = 0$ and 1.

From Eq. 3 we see if $R < .383\ \lambda$ then k_n'' will be imaginary making the wave damp out in the z direction as seen from Eq. 2. The amount of damping depends on how close to resonance the radius is. In Figure 3 v_R/A is graphed as a function of Z/λ. We see for the mode 0 the damping is less the closer R/λ is to the resonant value. We also see that the mode $n = 1$ for $R/\lambda = .38$ damps out more quickly than mode $n = 0$ even for R/λ as low as .22, about 40% lower than the resonant condition for that mode. We also see from Figures 1 and 2 that although the disc is being driven by a piston oscillating in the z direction the major motion can be radial.

From Eq. 6 we can also find the radial velocity as a function of r:

$$v_r = \sum_n \frac{2iA\, J_1(\alpha_n r/R)\, e^{i(k_n'' z - \omega t)}}{R\, k_n''\ J_1(\alpha_n)} \tag{12}$$

From Eq. 12 we see at $r = 0$ all modes are zero. For the $n = 0$ mode the maximum velocity occurs at about 75% of the maximum radius. A different situation would exist for an infinite strip of fluid between two planes. In that case the Bessel functions would be replaced by sin's and cos's and the maximum speed would occur at the fluid edge. For the $n = 1$ mode of oscillation the fluid for $r < .7R$ is out of phase with the outer section. Again the maximum speed for this mode does not occur at the edge but at about $r = .35R$.

B. Viscous Model

With the aid of the results we have obtained from Section IIA we may now proceed with a model closer to the physical system under study. Rather than an infinite column for the fluid we will assume a height H with the origin of Figure 1 moved along the z axis so the upper and lower boundaries occur at z = H/2 and -H/2 respectively. Since we are now including viscosity we will start with the Navier-Stokes equation:

$$\rho_o \left[\frac{\partial \vec{v}}{\partial t} + (\vec{v} \cdot \nabla)\vec{v} \right] = -c^2 \nabla\rho + \eta\nabla^2 \vec{v} + (\zeta + \frac{1}{3}\eta)\ \nabla\ (\nabla \cdot \vec{v}) \tag{13}$$

Since we are assuming the hydrodynamic variables may be expanded about their equilibrium values we will for now drop the higher order effects. We will take for a rectilinear coordinate system in component form:

$$\rho_o \frac{\partial v_i}{\partial t} = -c^2 \frac{\partial \rho}{\partial x_i} + \eta\nabla^2 v_i + (\zeta + \frac{1}{3}\eta) \frac{\partial}{\partial x_i} (\nabla \cdot \vec{v}) \tag{14}$$

If we operate on Eq. 2 with $\partial/\partial x_i$ and sum over i we have

$$\rho_o \frac{\partial \nabla \cdot \vec{v}}{\partial t} = -c^2 \nabla^2 \rho + \eta \nabla^2\ \nabla \cdot \vec{v} + (\zeta + \frac{1}{3}\eta) \nabla^2\ (\nabla \cdot \vec{v}) \tag{15}$$

The hydrodynamic variables must also obey the continuity equation:

$$\frac{\partial \rho}{\partial t} + \nabla \cdot (\rho \vec{v}) = 0 \tag{16}$$

where again to first order we have

$$\frac{\partial \rho}{\partial t} + \rho_o \nabla \cdot \vec{v} = 0 \tag{17}$$

Combining Eq's. 15 and 17 and assuming a time dependence $e^{i\omega t}$ we have

$$A_o \nabla^2 \rho = \rho \tag{18}$$

where

$$A_o = -\frac{i(\zeta + \frac{4}{3}\eta)}{\omega\rho_o} - \frac{c^2}{\omega^2} \tag{19}$$

The solution to Eq. 18 is

$$\rho = \sum_n \left[A_{1n} J_o (k_n r) e^{k_n'' z} + A_{2n} J_o (k_n r) e^{-k_n'' z}\right] e^{i\omega t} \tag{20}$$

where we have dropped the i from in front of the k_n'' factor since we will assume $R \leq .383\ \lambda$ and from Section IA we know for that case the z dependence is real. We also have analogous to Eq. 3

$$k^2 = k''^2 - \frac{1}{A_o} \tag{21}$$

In order to simplify the solution of the Navier-Stokes equation we define two new functions according to

$$v_r = \frac{\partial \phi}{\partial r} + \frac{\partial \psi}{\partial z} \tag{22}$$

and

$$v_z = \frac{\partial \phi}{\partial z} - \frac{1}{r} \frac{\partial}{\partial r} (r\psi) \tag{23}$$

Now we have

$$\nabla \cdot \vec{v} = \nabla^2 \phi\ ; \tag{24}$$

so from Eq's. 17 and 18 we find ϕ may be related to ρ:

$$\phi = - \frac{i\omega A_o \rho}{\rho_o} \tag{25}$$

The z component of Eq. 13 to first order is

$$\rho_o \frac{\partial v_z}{\partial t} = -c^2 \frac{\partial \rho}{\partial z} + \eta \nabla^2 v_z + \left(\zeta + \frac{1}{3}\eta\right) \frac{\partial (\nabla \cdot \vec{v})}{\partial z} \tag{26}$$

Using Eq's. 17, 18, 19, and 22 we obtain

$$\frac{\eta}{i\omega\rho_o} \nabla^2 \xi = \xi \tag{27}$$

where

$$\xi = \frac{1}{R} \frac{\partial}{\partial r} (r\psi)$$

Taking

$$k_n^2 = k_n'^2 - \frac{i\omega\rho_o}{\eta} \tag{28}$$

the solution of Eq. 27 we take to be

$$\xi = \sum_n \left[A_{3n} J_o (k_n r) e^{k_n' z} + A_{4n} J_o (k_n r) e^{-k_n' z} \right] e^{i\omega t} \tag{29}$$

From Eq. 28 then

$$\psi = \sum_n \left[A_{3n} J_1 (k_n r) e^{k_n' z} + A_{4n} J_o (k_n r) e^{-k_n' z} \right] e^{i\omega t}/k_n \tag{30}$$

Eq's. 20, 25 and 30 may be used with Eq's. 22 and 23 respectively to obtain

$$v_r = \sum_n \left(\frac{i\omega A_o k_n}{\rho_o} \left[A_{1n} e^{k_n'' z} + A_{2n} e^{-k_n'' z} \right] \right. \tag{31}$$

$$\left. + \frac{k_n'}{k_n} \left[A_{3n} e^{k_n' z} - A_{4n} e^{-k_n' z} \right] \right) J_1 (k_n r) e^{i\omega t}$$

and

$$v_z = \sum_n \left(\frac{-i\omega A_o k_n''}{\rho_o} \left[A_{1n} e^{k_n'' z} - A_{2n} e^{-k_n'' z} \right] \right. \tag{32}$$

$$\left. - \left[A_{3n} e^{k_n' z} + A_{4n} e^{-k_n' z} \right] \right) J_o (k_n r) e^{i\omega t}$$

Assuming a no-slip condition at $z = \pm H/2$ we must have $v_r = 0$ there. For the experiment we have performed $H/\lambda = .055$. From Figure 3 we see the amount of damping which has occurred as the wave traverses the vertical distance H of the disc. We will therefore take as an acceptable although not excellent approximation that $v_z = Ae^{-i\omega t}$ at $z = \pm H/2$. For these boundary conditions we find

$$A_{1n} = -A_{2n} = \frac{-2\rho_o k_n' A}{i\omega A k_n'' \alpha_n J_1 (\alpha_n) (2k_n' - k_n^2 H)} \tag{33}$$

$$A_{3n} = A_{4n} = \frac{2 k^2 HA}{\alpha_n J_1 (\alpha_n) (2k_n' - k_n^2 H) e^{k_n' H/2}} \tag{34}$$

For the case under study $k_n' >> k_n^2 H$ and $k_n'' H << 1$. If we assume we are near the mode 0 resonance condition from Figures 2 and 3 we see we may drop the higher modes. Under these approximations we have

$$v_r = \frac{Ak_o}{\alpha_o J_1(\alpha_o)} \left\{ -2z + \frac{H}{e^{k_o' H/2}} \left(e^{k_o' z} - e^{-k_o' z} \right) \right\} J_1(k_o r) e^{i\omega t} \tag{35}$$

$$v_z = \frac{2 A J_o(k_o r) e^{i\omega t}}{\alpha_o J_1(\alpha_o)} \tag{36}$$

From Eq. 28 we see that k_o' is complex. For v_z what actually occurs is a cos ωt rather than the exponential. For the radial component:

$$v_r = \frac{Ak_o}{\alpha_o J_1(\alpha_o)} \left\{ -2z + H \left[e^{R_e k_o' (z-H/2)} \cos \left[Im k_o' (z-H/2) + \omega t \right] \right.\right.$$

$$\left.\left. - e^{-R_e k_o' (z + H/2)} \cos \left[Im k_o' (z + H/2) + \omega t \right] \right] \right\} x \, J_1(k_o r)$$

By setting $r = R$ in the real form of v_r we may obtain a value of the radial amplitude of oscillation compared with that of the piston. For our sample we have $H = .032$ cm, $Re\ k' = Im\ k' = 1112/cm$ and at resonance $R = .22$ cm. The resulting ratio of radial velocity to maximum piston velocity (which equals also the ratio of radial distance amplitude to vertical piston distance amplitude) is plotted as a function of z in Figure 4. The resulting maximum ratio shows for our case the radial motion has an amplitude less than 20% that of for the piston. Therefore, the infinite ratio for mode 0 shown in Figure 2 turns out to be of the order of .1 when viscous effects are considered. Also in Figure 4 a diagram is shown which depicts the deformation of the disc cross section. As the planes move upward the fluid bulges out at the bottom and in at the top. As the planes then move downward the opposite occurs.

Let us now return to Eq. 13 and examine the term we omitted. In light of the solutions, Eq's. 35 and 36, we see that each term of Eq. 13 oscillates sinusoidally in time. Although in Eq's. 35 and 36 we have used the complex exponential form, since the velocity is real the term we earlier omitted from Eq. 13, $\rho_o \vec{v} \cdot \nabla\vec{v}$, will have a factor of $\cos^2 \omega t$. Since $\cos^2 \omega t = (1 + \cos 2\omega t)/2$ if the time average of the omitted term is taken a non-zero static value results. Therefore, the time average of the other terms in the equation must also give non-zero static values. Since these other terms involve only the hydrodynamic variables to the first power we conclude a static value must be added to the values we obtained in Eq's. 35 and 36. This static flow is called acoustic streaming. We will denote the static addition to the variables with a subscript 2 signifying the second order solution: v_{r2}, ρ_2, v_{z2}. The time average of Eq. 13 to second order is

$$\rho \langle \vec{v} \cdot \nabla v_r \rangle = -c^2 \frac{\partial \rho_2}{\partial r} + \eta \nabla^2 v_{2r} + (\zeta + \frac{1}{3}\eta) \frac{\partial}{\partial r} (\nabla \cdot \vec{v}_2) \tag{37}$$

$$\rho \langle \vec{v} \cdot \nabla v_z \rangle = -c^2 \frac{\partial \rho_2}{\partial z} + \eta \nabla^2 v_{2z} + (\zeta + \frac{1}{3}\eta) \frac{\partial}{\partial z} (\nabla \cdot \vec{v}_2) \tag{38}$$

where the brackets denote a time average and merely involve replacing the $\cos^2 \omega t$ factor with 1/2. If we operate on Eq's. 37 and 38 by $\partial/\partial z$ and $\partial/\partial r$, respectively, subtracting the results we obtain

$$\rho \left\langle \frac{\partial}{\partial z} (\vec{v} \cdot \nabla v_r) - \frac{\partial}{\partial r} (\vec{v} \cdot \nabla v_z) \right\rangle = \eta \left[\frac{\partial}{\partial z} \nabla^2 v_{2r} - \frac{\partial}{\partial r} \nabla^2 v_{2z} \right] \tag{39}$$

Again invoking the approximations used to obtain Eq's. 35 and 36 along with $k_o' H >> 1$ we find we may identify ∇^4 with $\partial^4/\partial z^4$ and obtain with the help of Eq's. 22 and 23

$$\psi_2 = \frac{\rho A^2 k_o^3 J_1(k_o r)}{2\eta \alpha_o^2 J_1(\alpha_o)} \cdot \frac{\partial J_1(k_o r)}{\partial (k_o r)} \left\{ - \frac{z}{4(R_e k_o')^3} \right. \tag{40}$$

$$\left. \times \left[e^a(\cos a - \sin a) + e^{-b}(\cos b + \sin b) \right] + c_1 z^3 + c_2 z^3 + c_3 z + c_4 \right\}$$

where

$$a = \mathrm{Re}\ k_o' \ (z - H/2) \tag{41}$$

$$b = \mathrm{Re}\ k_o' \ (z + H/2) \tag{42}$$

and where we have again taken the real part assuming Re k_o' = Im k_o' as we find to be approximately true for our systems. The contribution from ϕ_2 can be shown to be small so that Eq's. 22 and 23 become

$$v_{2r} = \partial\psi/\partial z \tag{43}$$

$$v_{2z} = -\frac{1}{r}\frac{\partial}{\partial r}(r\psi_2)$$

The values of the C_i's may be found using the boundary conditions that both v_{2r} and v_{2z} equal zero at $z = \pm H/2$. Finally we obtain the second order contributions to the velocity:

$$v_{2r} = -\frac{\rho A^2 k_o^3 H J_1(k_o r)}{\eta \alpha_o^2 J_1^2(\alpha_o)} \cdot \frac{\partial J_1(k_o r)}{\partial(k_o r)} \left\{ \frac{z}{2(\mathrm{Re}\ k_o')^2} \left[e^{a} \sin a + e^{-b} \sin b \right] - \frac{3z^2}{2(\mathrm{Re}\ k_o')^3 H^2} + \frac{3}{8(\mathrm{Re}\ k_o')^3} \right\} \tag{44}$$

$$v_{2z} = -\frac{\rho A^2 k_o^3}{2\eta \alpha_o^2 J_1^2(\alpha_o)} \frac{1}{r}\frac{\partial}{\partial r}\left(r J_1(k_o r) \frac{\partial J_1(k_o r)}{\partial (k_o r)} \right)$$

$$\times \left\{ -\frac{z}{4(\mathrm{Re}\ k_o')^3} \left[e^{a}(\cos a - \sin a) + e^{-b}(\cos b + \sin b) \right] + \frac{3z}{8(\mathrm{Re}\ k_o')^3} - \frac{z^3}{2(\mathrm{Re}\ k_o')^3 H^2} \right\} \tag{45}$$

Eq's. 44 and 45 will be the basis of a comparison with the experimental results we have obtained.

III. EXPERIMENT

A barium titanate crystal was used to produce the ultrasonic wave (cw) in the sample under study. The wave was transmitted from the crystal through the conducting glass electrode immediately above the crystal, through vacuum grease which was used to mount the sample holder, through the bottom glass slide, through the sample fluid disc, and on through the upper glass slide. Various fluids were used: water, a cholesteric liquid crystal, a nematic liquid crystal and a transparent vegetable oil. The oil's viscosity is closer to the nematic whose motion we will ultimately consider. Therefore, measurements reported here concern the velocity induced in the oil. To measure the magnitude of the flow in the disc the oil was doped with a hydrocarbon base ferrofluid (0.1% concentration). Aggregates of magnetite can then be seen in the oil by means of a polarizing microscope. By measuring the speed of these particles the speed of the oil may be determined. The particles were of the order of one micron in diameter. The thickness of the disc was .032 cm so the particle size was small compared to the distance over which the speed of the fluid changed appreciably. The diamter of the disc was from one to four mm, small compared to the 12.7 mm diameter of the barium titanate crystal. The microscope was calibrated so the vertical position of the particle whose speed was being measured could be determined when the microscope was focused on that particle. A sealed container was also used so that the ultrasonic wave would first travel through one cm of water before reaching the fluid disc. Using a capillary viscometer the ratio of viscosity to density of the oil was determined, $\eta/\rho = 0.66 \pm 0.03$ cm^2/sec. From Eq. 28 we see k_o' can now be determined if we know the frequency and wave speed. We take $c = 1.46 \times 10^5$ cm/sec and $f = .26$ MHz. We find the real part of $k_o'^2$ small so $k_o' = 1112\ (1 + i)$/cm.

From Eq. 44 we see that the radial flow goes to zero at r = 0 due to the $J_1(k_o r)$ factor. It becomes larger for larger values of r and then goes to zero near the edge r = R due to the derivative of $J_1(k_o r)$. The value of v_{2z} on the other hand is larger at r = 0 and decreases as r is increased and finally is larger but with a different sign near r = R. A diagram of the flows our equations predict is shown in Figure 5. The upper diagram, I, depicts the flow pattern although actually H is much smaller with respect to R than we have drawn. The lower pattern is not what we predict from our equations but the flow patterns that would pertain if the models proposed by other authors were applicable. If the fluid is observed at r = R/2 as one focuses from the top to the bottom the particles can be seen to flow toward the center near the top, toward the edge near the middle and toward the center near the bottom, in accordance with the pattern I which our equations predict. A more quantitative comparison is presented in Figure 6. The graph shows the fluid speed in the radial direction (toward the center is taken as positive) as a function of z. For the data shown $R/\lambda = .21$ and the frequency was .26 MHz. The taller (labeled I) peaked curve in Figure 6 is the best fit of the quantity in brackets in Eq. 44 using our experimentally determined value for k'_o. Since everything in the brackets is determined a best fit was made of the data to a constant times the bracket. The constant so determined was $(13 \pm 1) \times 10^9$ cm^3 sec/micron and $\chi^2 = 2.3$. The smaller peaked curve (labeled II) in Figure 6 is a best fit where both k'_o and the constant are to be found. Their values are respectively 470 ± 10/cm and $2.0 \pm 0.1 \times 10^9$ cm^3 sec/micron with $\chi^2 = 0.3$. The later value of k'_o appears unacceptable in light of the small error on viscosity and the better fit we take to be fortuitous. It is noteworthy that the fit is so good since for the data plotted R/λ is about half of the resonant value for which Eq. 44 was derived. Notice the peak near the top of the disc, the one on the

right in Figure 6, is slightly less than the one on the left. The reason for the difference has to do with our assumption that $v_z = Ae^{i\omega t}$ both at the top and bottom of the disc. Making the boundary condition that $v_z = 0$ at the top decreases the top peak to about 20% of the bottom peak. The data seems to be in between these two extremes and it would appear we have taken the better approximation in allowing the upper boundary to move. Data was taken for R/λ equal to .21, .29, .30, .36, .39, and .45. All of the radial velocity profiles have the same basic pattern as those data shown in Figure 6.

Frequencies of .26, .77, .68, and 1.07 MHz were used both for direct contact of the sample holder with the barium titanate crystal and with the crystal in a cell so that the wave was propagated through about one cm of water before reaching the sample. All of the flow patterns observed in the microscope using the water cell were radial. For the direct contact case for certain frequencies and locations on the crystal it was possible to induce patterns of either two or four rather circular flow patterns. The discs became slightly distorted from circular to ellipsoidal in shape for these non-radial patterns. These patterns are assumed due to non-uniform oscillation of the crystal. For these cases the pressure in Eq. 1 must be assumed to be a function of angle. The solutions are similar to the well studied oscillating drumhead.

The radial velocity in Eq. 44 is proportional to A^2, the square of the piston velocity amplitude. But this amplitude should be proportional to the voltage applied to the barium titanate crystal. In Figure 7 therefore we have plotted the radial velocity measured at a fixed r and z as a function of voltage. The solid line is a fit to a voltage square curve.

REFERENCES

1. V. Vzolina, Trudy Lomonosov Inst. Akad. Nauk SSSR 8, 11 (1936)
2. J.L. Fergason, Proc. Second International Symposium on Acoustic Holography, 2, 53 (1970).
3. L.W. Kessler and S.P. Sawyer, Appl. Phys. Lett. 17, 440 (1970).
4. W. Helfrich, Phys. Rev. Lett. 29, 1583 (1972).
5. P. Greguss, Acustica 29, 52 (1973).
6. J.F. Dreyer, J. Acoust. Soc. Am. 55, 407 (1974).
7. C. Sripaipan, C.F. Hayes and G.T. Fang, Sixth International Liquid Crystal Conference, J-29 (1976).

   C. Sripaipan, C.F. Hayes and G.T. Fang, Phys. Rev. 15A, 1297 (1977).
8. S. Candau, A. Peters and S. Nagai, Sixth International Liquid Crystal Conference J-30 (1976).
9. J.L. Dion and F. DeForest, Sixth International Liquid Crystal Conference, K-18 (1976).
10. C.F. Hayes, Liquid Crystals and Ordered Fluids, 3, 287 (1978).
11. S. Nagai and K. Iizuka, Mol. Cryst. Liq. Cryst. 45, 83 (1978).
12. S. Nagai and Kozo Iizuka, Japan. J. Appl. Phys. 17, 723 (1978).

Figure 1. Diagram for calculations of the infinite non-viscous cylindrical fluid. The piston driving the oscillations is in the xy plane. For the viscous disc of height H the origin is moved along the z axis a distance H/2.

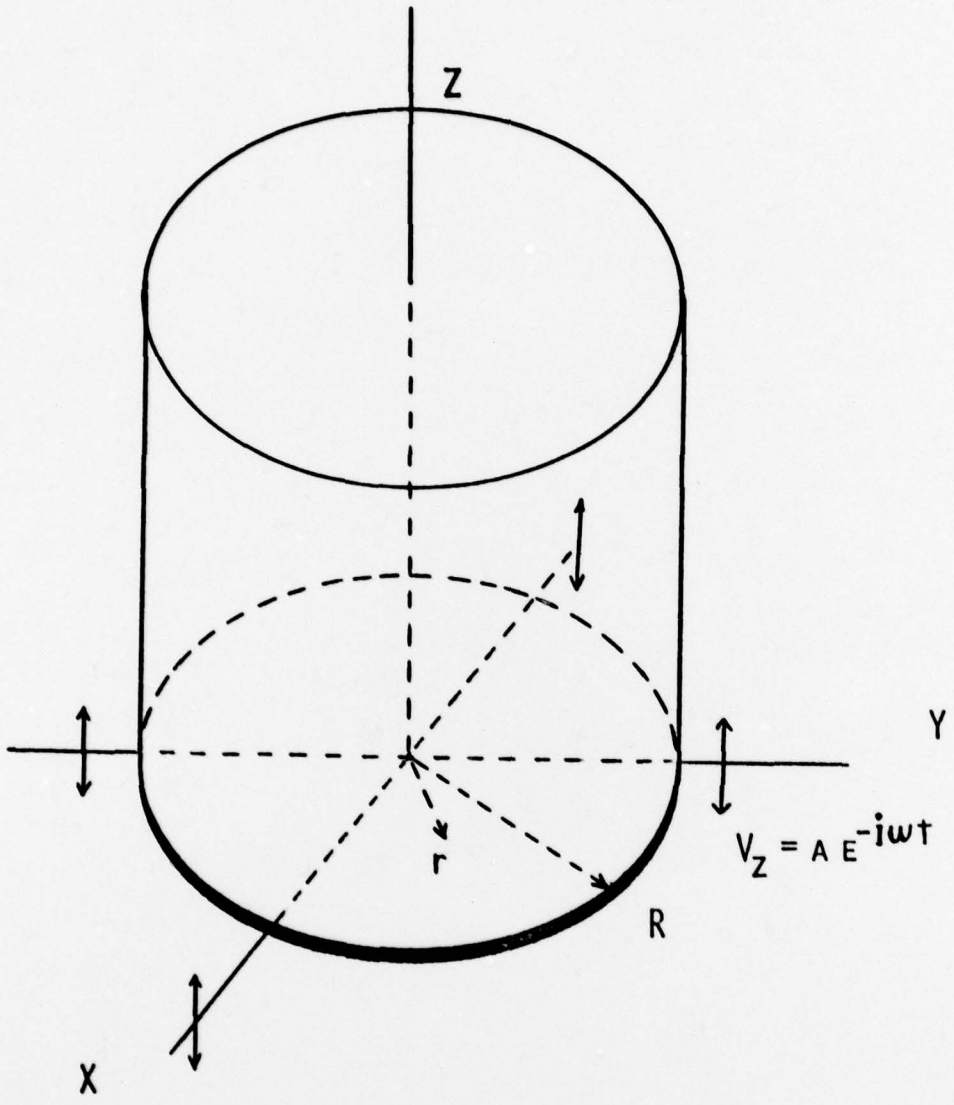
Z
Y
X
r
R
$V_Z = A E^{-i\omega t}$

Figure 2. Graph for the ratio of radial speed amplitude to piston speed amplitude versus the ratio of cylindrical radius to acoustic wavelength.

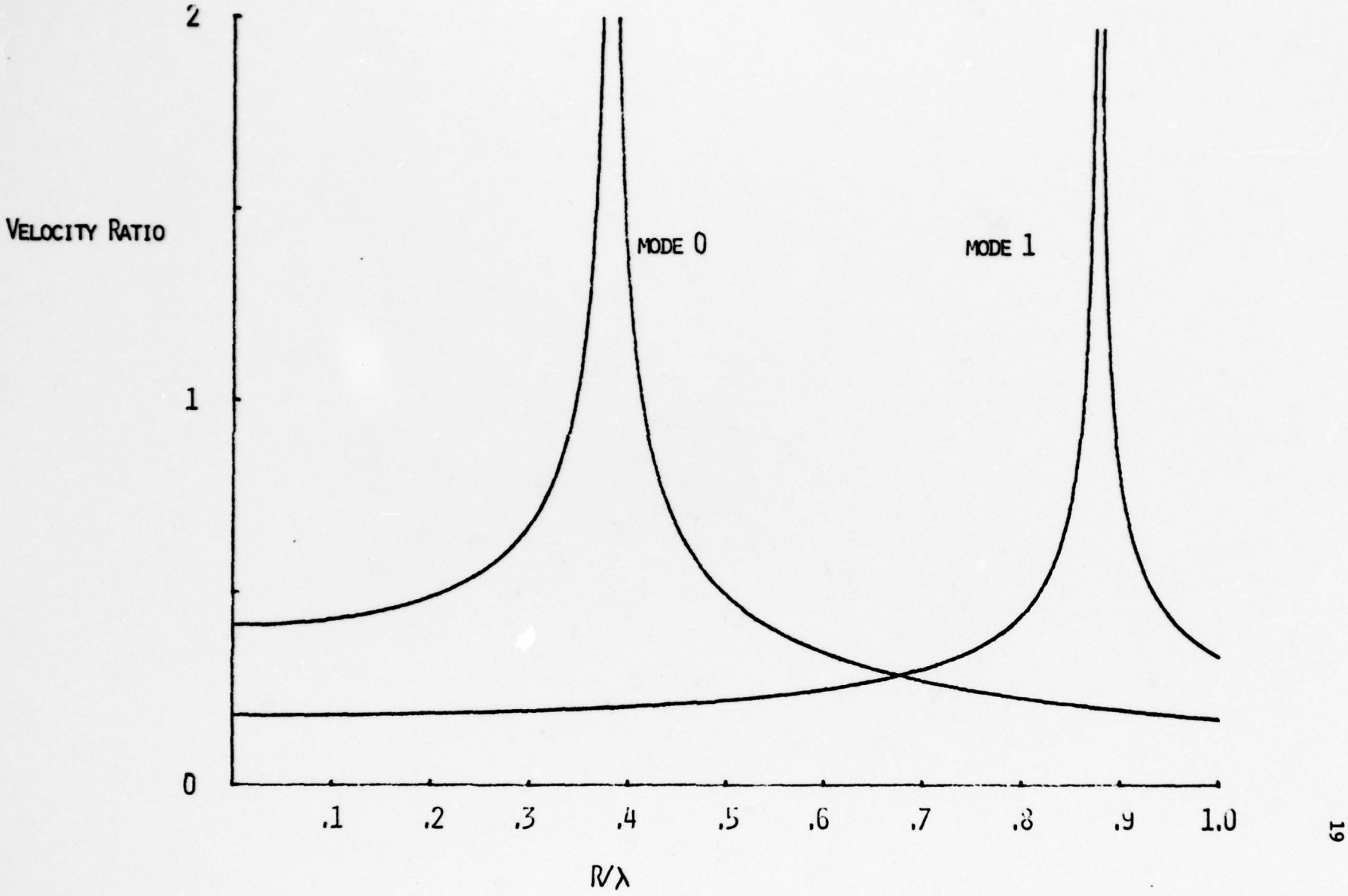
VELOCITY RATIO
2
1
0
MODE 0
MODE 1
.1
.2
.3
.4
.5
.6
.7
.8
.9
1.0
R/λ

Figure 3. Graph of velocity ratio versus z/λ. The velocity ratio is the ratio of radial speed amplitude to piston speed amplitude.

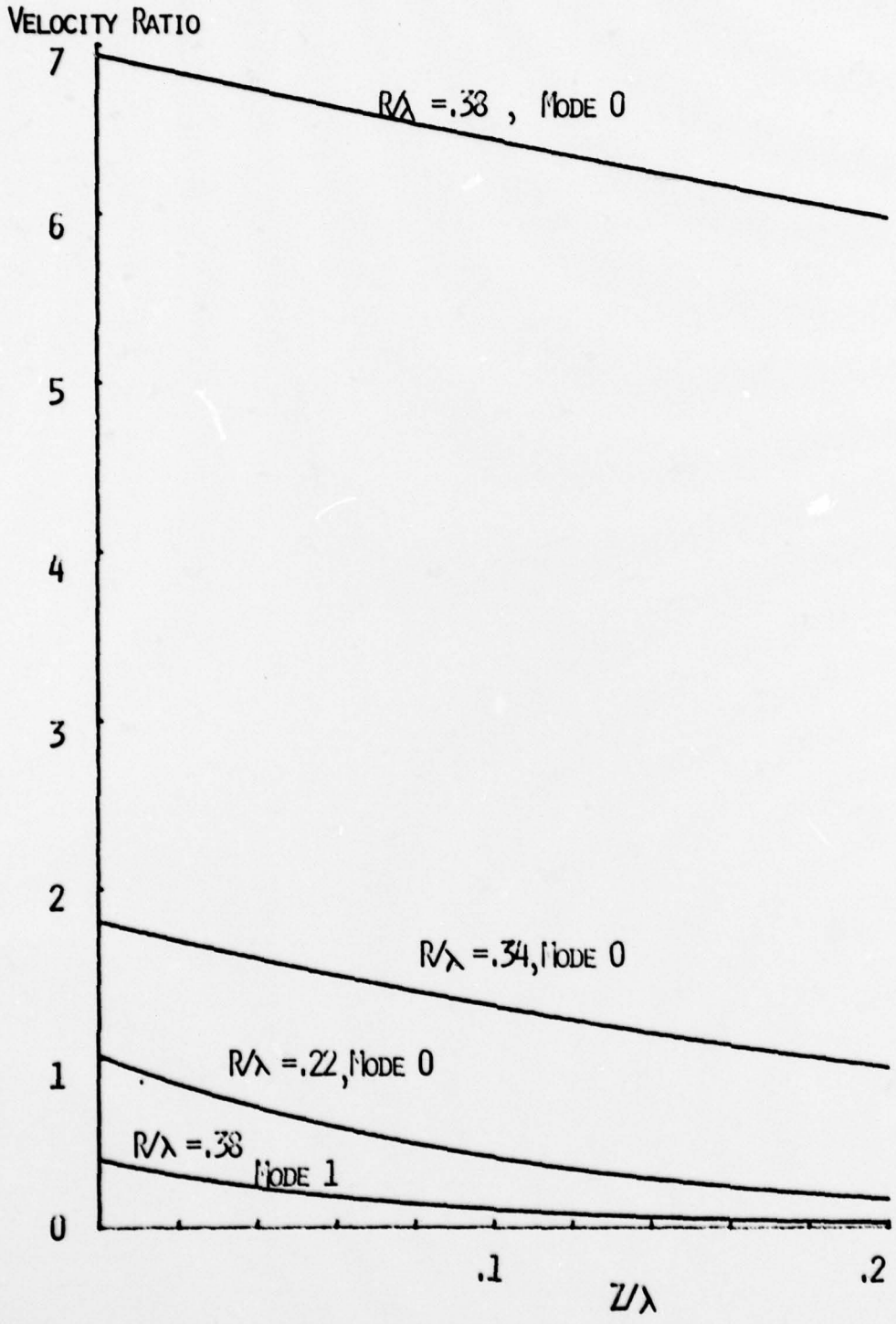
VELOCITY RATIO
7
6
5
4
3
2
1
0
R/λ =.38 , MODE 0
R/λ =.34, MODE 0
R/λ =.22, MODE 0
R/λ =.38 MODE 1
.1
.2
Z/λ

Figure 4. Velocity ratio (radial to piston's) versus distance along the z axis. The model assumes no-slip at the boundaries and incorporates viscosity.

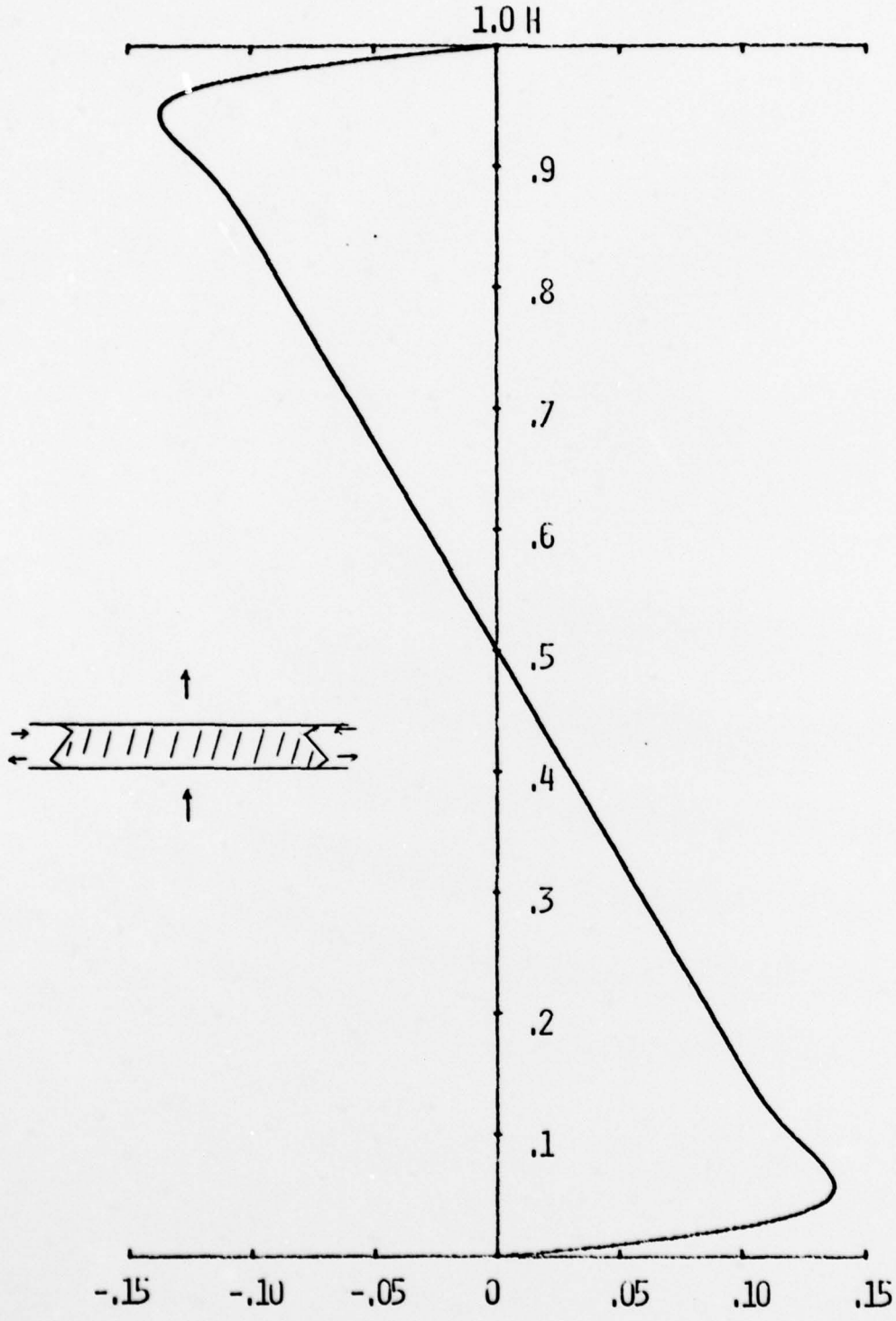
1.0 H
.9
.8
.7
.6
.5
.4
.3
.2
.1
-.15
-.10
-.05
0
.05
.10
.15
VELOCITY RATIO

Figure 5. Flow patterns in the disc due to acoustic streaming. The upper diagram, I, is the pattern predicted from our second order solutions. The lower pattern, II, is that assumed in other theories.

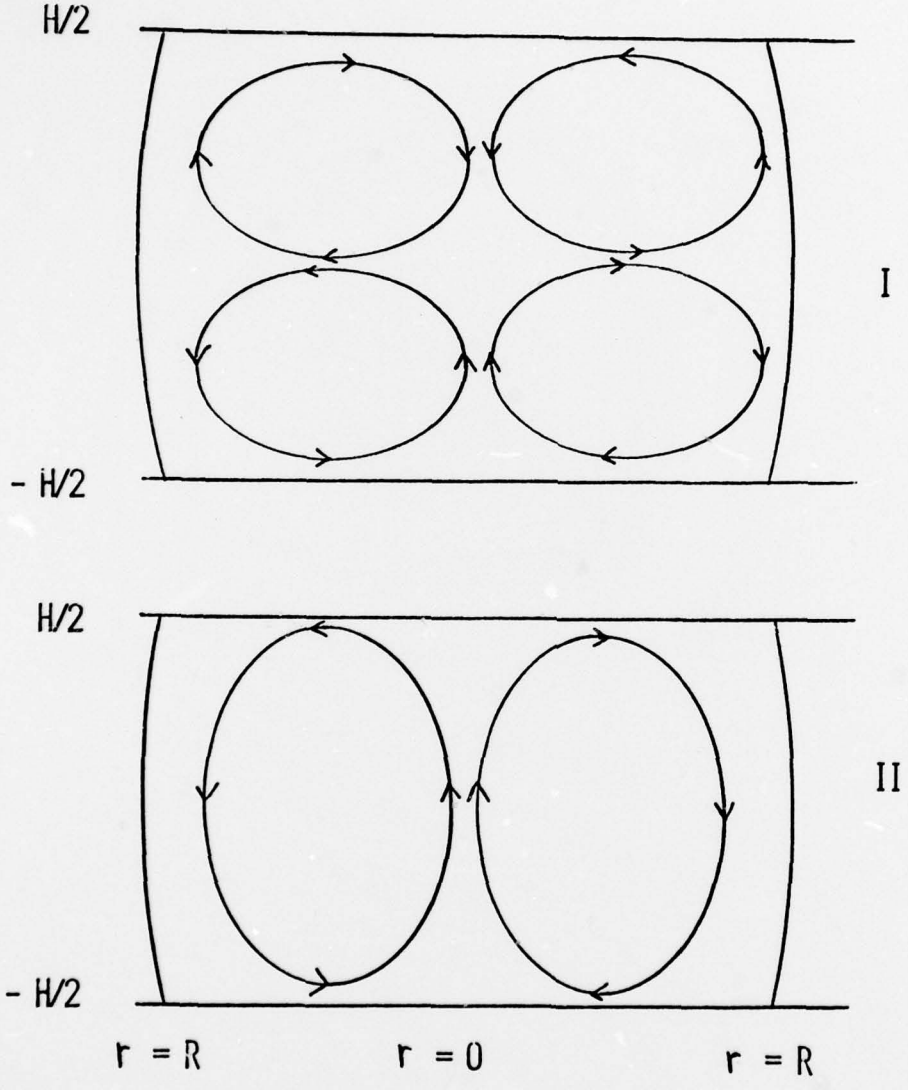
H/2
- H/2
I
H/2
- H/2
II
r = R
r = 0
r = R

Figure 6. Velocity of fluid due to acoustic streaming versus distance through the disc at r = R/2. Curve I is a best fit to the data using our measured value of k'_o. Curve II is a best fit allowing k'_o to be determined by the fitting process itself.

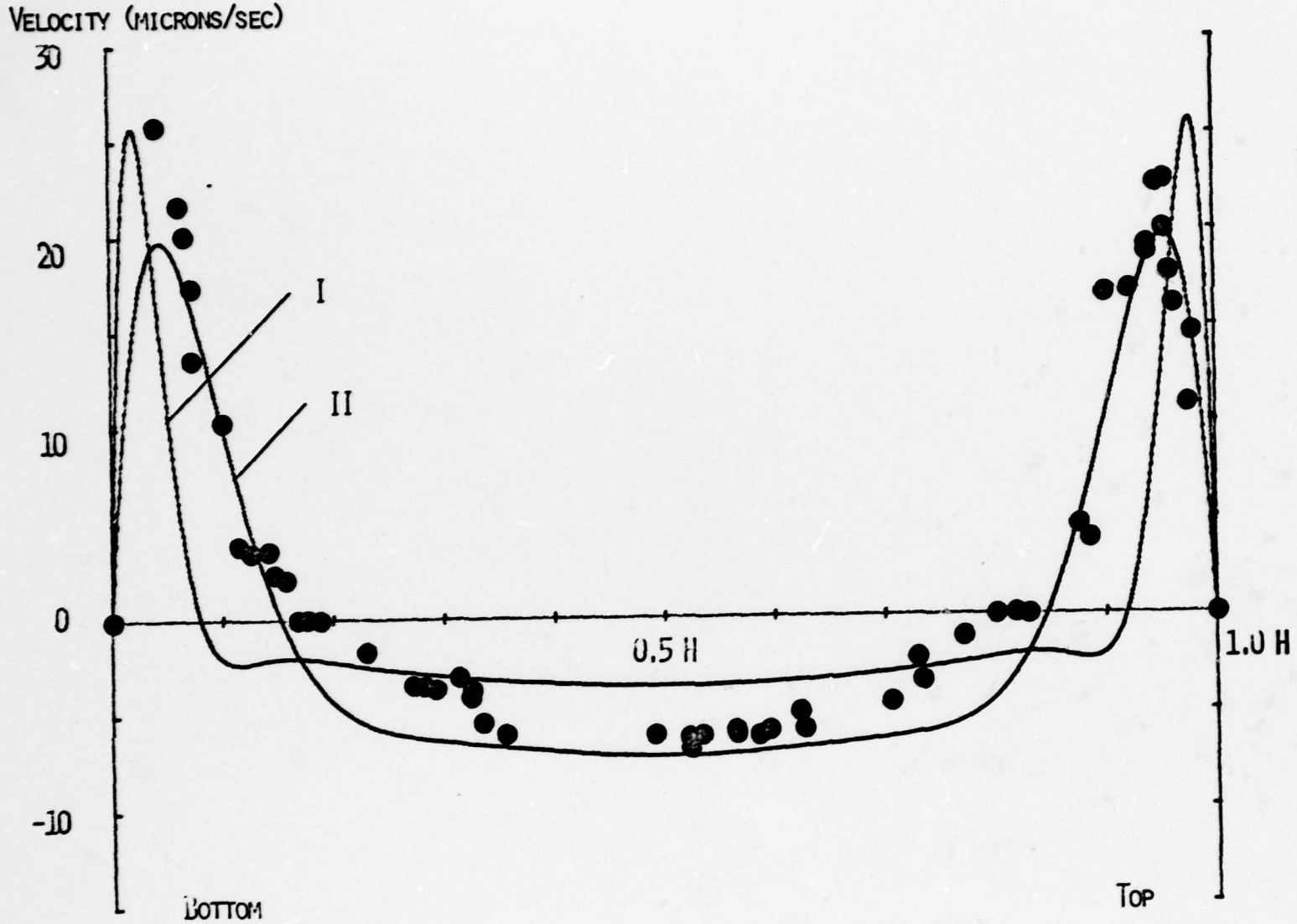
VELOCITY (MICRONS/SEC)
30
20
10
0
-10
I
II
0.5 H
1.0 H
BOTTOM
TOP

Figure 7. Velocity of the fluid due to acoustic streaming versus voltage applied to the transducer. The solid line is a best fit to a voltage square dependence.

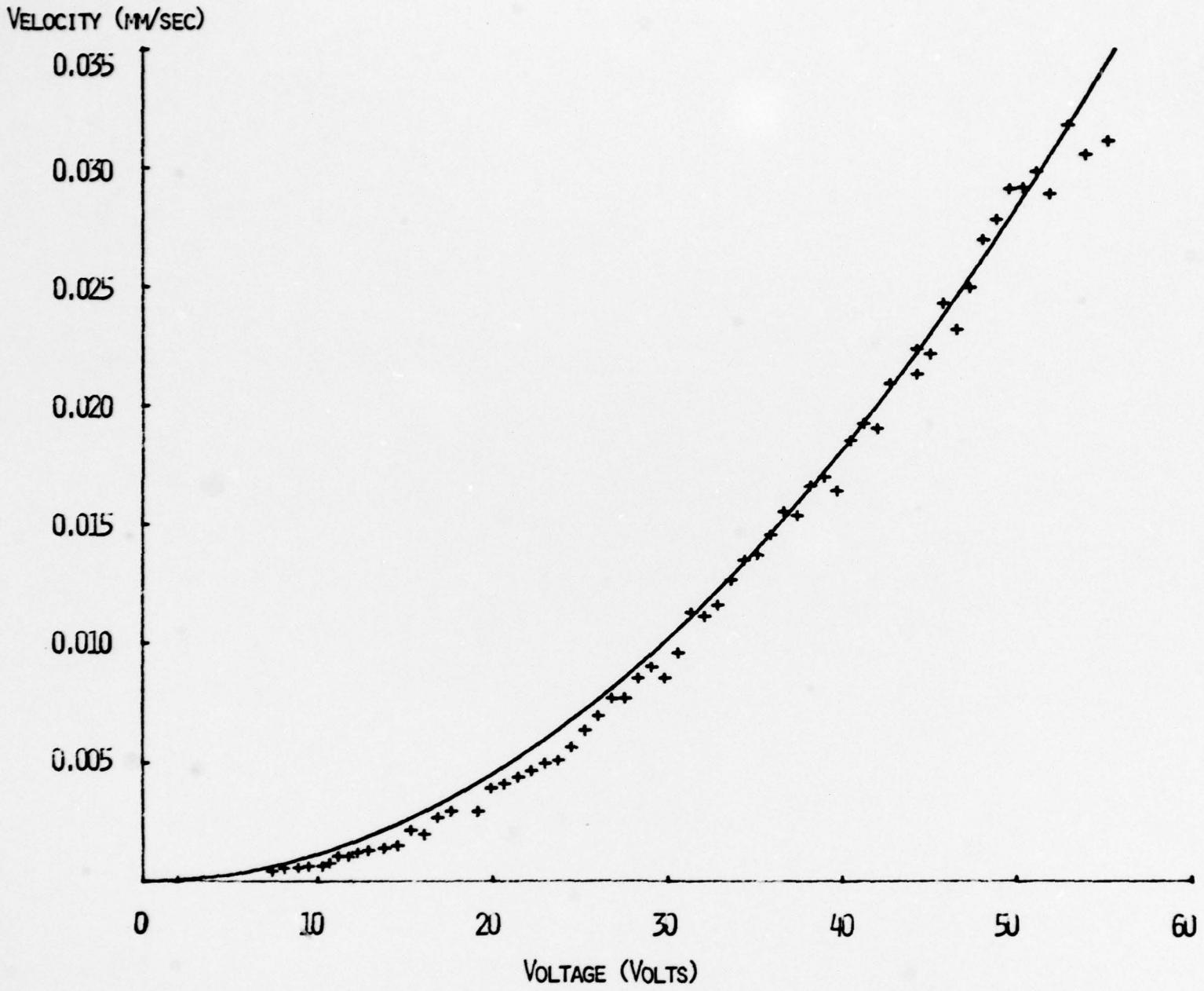
VELOCITY (MM/SEC)
0.035
0.030
0.025
0.020
0.015
0.010
0.005
0
10
20
30
40
50
60
VOLTAGE (VOLTS)